

## Stability of Laminated Rubber Bearing and Its Application to Seismic Isolation

Gyeong-Hoi Koo\*, Jae-Han Lee\*, Hyeong-Yeon Lee\* and Bong Yoo\*

(Received December 28, 1998)

In this paper, the effects of shape factors on the buckling loads in the laminated rubber bearing (LRB) are investigated to guide the design of LRB in determination of the rubber plate thickness and the total rubber height. To substantiate the application of LRB to the seismic isolation of nuclear power plants, the seismic analyses and shaking table tests are carried out for a seismically isolated structure using four LRBs. The parameter equations of seismic isolation frequency are obtained from the shaking table tests and the quasi-static tests of LRB itself to investigate the effects of the LRB characteristics in prediction of maximum peak acceleration responses by analysis. From the comparison of the maximum peak acceleration responses obtained from numerical analyses and experiments, it is verified that the horizontal stiffness variations of LRB should be considered in seismic analysis to get more accurate results.

**Key Words:** the Laminated Rubber Bearing(LRB), Seismic Isolation Desgn, Stability, Buckling Load

### Nomenclature

<p><math>A_s</math> : Shear area</p> <p><math>C_i^H, C_i^V</math> : Horizontal and vertical viscous damping of <math>i</math>th LRB</p> <p><math>D_o, D_i</math> : Outer and inner diameter of rubber plate</p> <p><math>E_b</math> : Apparent bending modulus</p> <p><math>\bar{E}_b</math> : Modified bending modulus</p> <p><math>E_o</math> : Young's modulus of elasticity</p> <p><math>E_\infty</math> : Bulk modulus</p> <p><math>F_i^H, F_i^V</math> : Horizontal and vertical restoring force of <math>i</math>th LRB</p> <p><math>f_{iso}</math> : Seismic isolation frequency</p> <p><math>G</math> : Shear modulus</p> <p><math>I_n</math> : Moment of inertia of <math>n</math>th floor</p> <p><math>K_{eq}</math> : Equivalent shear stiffness of LRB</p> <p><math>K_i^H, K_i^V</math> : Horizontal and vertical stiffness of <math>i</math>th LRB</p> <p><math>l</math> : Total height of LRB</p> <p><math>M</math> : Total mass of superstructure</p> <p><math>n_R</math> : Number of rubber layer</p> <p><math>P</math> : Vertical load</p>	<p><math>P_B</math> : Buckling load</p> <p><math>P_E</math> : Euler buckling load</p> <p><math>S_1, S_2</math> : Shape factors</p> <p><math>S_b</math> : Bending stiffness</p> <p><math>t_R, t_s</math> : Thickness of rubber and steel plate</p> <p><math>T_R</math> : Total height of rubber plate</p> <p><math>k</math> : Hardening constant of rubber</p> <p><math>\theta_G</math> : Rotational angle at mass center</p>
--	--

### 1. Introduction

Recently, the seismic isolation design using the laminated rubber bearing (LRB) has received considerable attention due to its wide application to nuclear power plants, buildings, and industrial structures.

In general, the LRB is a composite structure laminated with thin rubber plates and steel plates. Due to the structural rigidity in vertical direction, the LRB can support heavy weights. However, this is horizontally very flexible to make the superstructures almost rigid body motion when the earthquake is occurred.

\* Korea Atomic Energy Research Institute Taejon, Korea

For the realization of LRB applied to very heavy structures such as nuclear power plants for seismic isolation, it is important to consider the stability of LRB at the basic design stage to ensure the global safety of seismically isolated structure. In the design of LRB, the rubber plate thickness and total rubber height, i. e. the number of rubber plates should be carefully determined with consideration of stability because these design parameters principally affect the changes of vertical buckling loads. Many researchers have investigated the stability of LRB using experiments and several mathematical models (Haringx, 1948; Gent, 1964; Koh and Kelly, 1987; Koo et al., 1998). In this paper, the stability equations of LRB are investigated and are expanded with parameters such as the number of the rubber plate and the rubber thickness in case of with and without consideration of the rubber compression effects. From the derived parametric equations, the effects of shape factors on the buckling loads of LRB are investigated to guide the design of LRB in determination of the rubber plate thickness and the total rubber height.

To investigate the seismic isolation performance, the shaking table tests and the numerical analyses are carried out for a seismically isolated structure using four LRBs. Actually, LRB has a complicated horizontal stiffness characteristics such as wind load control stiffness, earthquake control stiffness, and ultimate strain control stiffness in range of cyclic shear strains (Forni et al., 1994). And the characteristics of horizontal stiffness are also affected by the loading rates, i. e. excitation frequencies (Koo and Ohtori, 1998). Therefore, the seismic isolation frequency may be changed as the earthquake level increases. In this paper, seismic time history analysis for a seismically isolated structure is carried out to investigate the effects of the seismic isolation frequency changes on earthquake responses. To consider the changes of the seismic isolation frequency in analyses, the parameter equations of the seismic isolation frequency for maximum cyclic shear displacements of LRB are obtained from the shaking table tests, i. e. considering fast excitation, and from the quasi-static tests of LRB itself,

i. e. considering slow excitation. The comparison of the maximum peak acceleration responses obtained from analyses and experiments are performed to verify the importance of horizontal stiffness changes of LRB in seismic analysis.

## 2. Stability of the Laminated Rubber Bearing

### 2.1 Review of stability equations

In general, as shown in Fig. 1, with assumption of small displacement and linear theory, the horizontal stiffness of LRB is represented by (Haringx, 1948)

$$K_H = \frac{P^2}{2qS_b \tan(ql/2) - Pl} \quad (1)$$

where

$$q^2 = \frac{P}{S_b} \left( 1 + \frac{P}{S_s} \right) \quad (2)$$

$P$  is the vertical load applied to end plate of LRB, and  $l$  is the total height of LRB including the rubber plates and steel plates.

In Eq. (2), the bending and shear rigidity,  $S_b$  and  $S_s$  are expressed as follows;

$$S_b = \bar{E}_b I / n_{RT} \quad (3)$$

$$S_s = GA_s l / n_{RT} \quad (4)$$

where

$$l = n_{RT} t_R + (n_R - 1) t_S \quad (5)$$

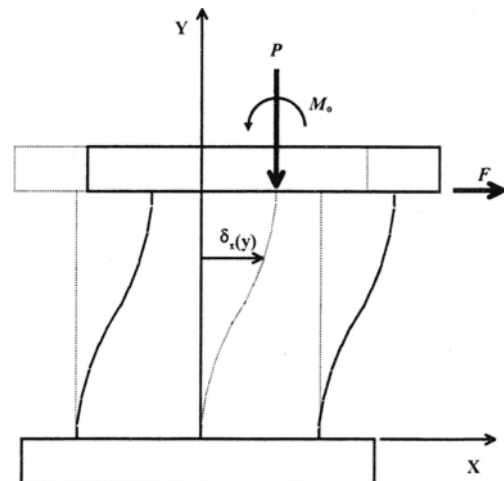


Fig. 1 Assumed displacement shape of LRB subjected to end loads.

$$\bar{E}_b = E_b E_\infty / (E_b + E_\infty) \quad (6)$$

$$E_b = E_o \left( 1 + \frac{2}{3} k S_1^2 \right) \approx 3G \left( 1 + \frac{2}{3} k S_1^2 \right) \quad (7)$$

In Eqs. (3) to (5),  $n_R$ ,  $t_R$  and  $t_s$  represent a number of rubber plate, thickness of rubber and steel plate respectively.  $\bar{E}_b$  is the elastic modulus for bending of the unit rubber plate, in which both end surfaces are rigidly constrained, with consideration of rubber compression effects (Fujita et al., 1987). The symbols used in above equations are expressed in Nomenclature.

To investigate the stability of LRB for vertical loads, we can consider the buckling load to make the horizontal stiffness zero. This condition is simply obtained when we put the denominator of Eq. (1) as infinite value. Therefore, the buckling load should satisfy the following condition obtained from  $\tan(ql/2)$  in Eq. (1).

$$ql = \pi \quad (8)$$

After substituting Eq. (8) to Eq. (2), the characteristic equation for the buckling load,  $P_B$ , is obtained as follows;

$$P_B^2 + S_s P_B - \frac{\pi^2 S_b S_s}{l^2} = 0 \quad (9)$$

From Eq. (9), the vertical buckling load of LRB can be expressed as follows;

$$P_B = \frac{S_s}{2} \left[ \left( 1 + \frac{4P_E}{S_s} \right)^{1/2} - 1 \right] \quad (10)$$

where

$$P_E = \pi^2 S_b / l^2 \quad (11)$$

which is called as the Euler buckling load in case of no shear displacement of LRB.

For a typical LRB, it is known that PE is greater than  $S_s$ . Therefore the equation of the buckling load in Eq. (10) can be simplified as follows;

$$P_B = \sqrt{P_E S_s} \quad (12)$$

## 2.2 Investigation of shape factors effects

From Eq. (12), we can see that the buckling load depends on the total height of LRB, the number of rubber plates, and the rubber thickness, i. e. geometric shape of LRB. For a circular type of LRB, the shape factors are often used to

represent the index of a geometric stability.

In general, the shape factors of LRB for circular sectional type are defined as follows;

$$S_1 = (D_o - D_i) / (4t_R) \quad (13)$$

$$S_2 = D_o / n_R t_R \quad (14)$$

As expressed in Eqs. (13) and (14), shape factors,  $S_1$  and  $S_2$  indicate the effect of rubber plate thickness,  $t_R$  and total rubber height,  $n_R t_R$  respectively. Actually in design of LRB, it is very important to determine the rubber plate thickness and total rubber height, i. e. shape factors, with consideration of stability. From Eq. (12), we can discuss the shape factor effects on the buckling load.

In case of neglecting the rubber compression effects, i. e. in Eq. (3) is replaced with Eb. After substituting Eqs. (3), (4), (7), (11), and (13) to Eq. (12), and arranging some items, it is found that the buckling load is directly proportional to

$$P_B \propto \left( \frac{1}{n_R t_R^2} \right) \quad (15)$$

In above Eq. (15), when  $S_2$  is constant, i. e. considering constant total rubber height.  $n_R t_R =$  constant, the buckling load proportionally decreases as the rubber plate thickness increases. And when  $S_1$  is constant, i. e.  $t_R =$  constant, the buckling load proportionally decreases as the number of rubber plates increases. Therefore, we can see that the shape factors,  $S_1$  and  $S_2$  affects the buckling load with same ratio in case of no rubber compression effects.

However, in the case of considering the rubber compression effects, the buckling load is proportional to

$$P_b \propto \left\{ \frac{1}{t_R^2 + 1/c} \right\}^{1/2} \left( \frac{1}{n_R t_R} \right) \quad (16)$$

where  $c$  is a constant resulted from rubber compression effects. In above Eq. (16), when  $S_1$  is constant, the buckling load proportionally decreases as the number of rubber plates increases. But when  $S_2$  is constant and the rubber plate thickness increases, the ratio of the buckling load decreasing is smaller than the case of no consideration of rubber compression effects due to a constant,  $c$ .

In conclusion, with considering the rubber

compression effects, the ratio of increasing the total rubber height affects the decrease of the buckling load more than that of increasing the rubber plate thickness.

For example of application, Fig. 2 and Fig. 3 show the sensitivity of the buckling load for shape factor variations. The data of LRB used in examples of application are;  $D^o=45\text{cm}$ ,  $D^i=0.0\text{cm}$ ,  $G=0.82\text{ MPa}$ ,  $E_o=2.46\text{ MPa}$ ,  $E_\infty=1.47\text{ GPa}$ , and  $k=0.5$ . Fig. 2 shows the effect of the rubber plate thickness on the buckling load in case of  $S_2=6$ , i. e. considering constant total rubber height with changes of rubber plate thickness and total number of rubber plates. Fig. 3 shows the effect of total rubber height on the buckling load in case of

$S_1=45$ , i. e. considering constant rubber plate thickness,  $t_R=2.5\text{ mm}$  with change of total number of rubber plates. From both figures, it is verified that decrease of shape factor,  $S_2$  induces more reduction of the buckling load than shape factor,  $S_1$ .

### 3. Application of LRB to Seismic Isolation

#### 3.1 Formulation of a seismically isolated structure (SIS)

##### 3.1.1 Rigid body model

In general, a seismically isolated structure, which adapts the laminated rubber bearings, can be assumed to represent the rigid body motion due to its fundamental frequency shift. For simple modeling of SIS shown in Fig. 4(a), the general equations of motion for base excitation problem using rigid body model shown in Fig. 4(a) can be expressed as follows;

$$m\ddot{x}_G + \sum_{i=1}^N F_i^H = -m\ddot{x}_g \tag{17}$$

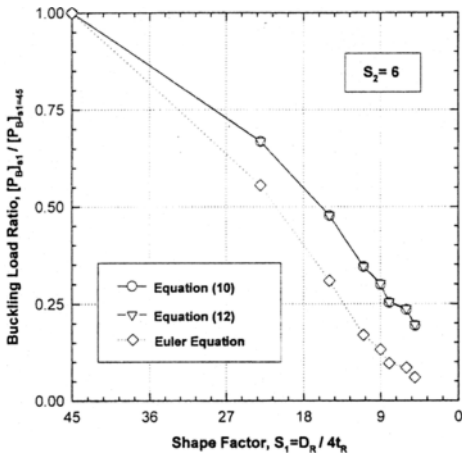


Fig. 2 Shape factor,  $S_1$  effects on buckling loads of LRB.

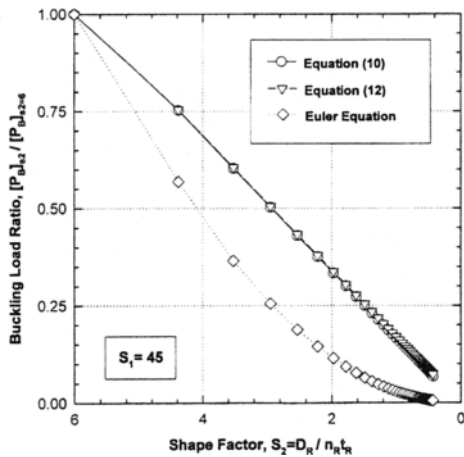
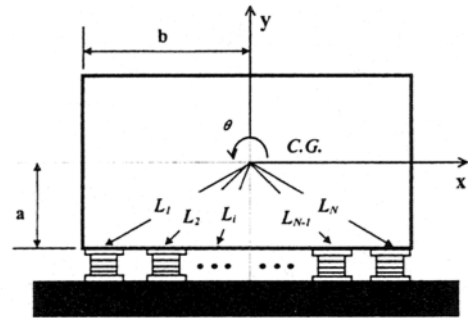
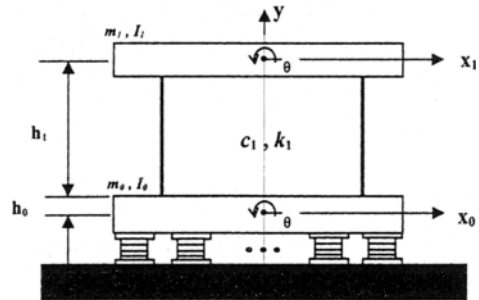


Fig. 3 Shape factor,  $S_2$  effects on buckling loads of LRB.



(a) Rigid body model



(b) Multi-d.o.f. model

Fig. 4 Mathematical model for numerical analyses.

$$m\dot{y}_G + \sum_{i=1}^N F_i^y = -m\dot{y}_g \quad (18)$$

where  $m$ ,  $\dot{x}_g$  and  $\dot{y}_G$  are total mass of superstructure, input ground acceleration, horizontal and vertical acceleration response vectors at mass center, and  $N$ ,  $F_i^H$  and  $F_i^y$  represent a number of LRB used in analysis, horizontal and vertical restoring force of  $i$ th LRB respectively.

The rotational equation of motion considering rocking motion can be expressed as follows;

$$\begin{aligned} I\ddot{\theta}_G + \sum_{i=1}^{N_L} F_i^H L_i \sin(\alpha_i + \theta_G) \\ + \sum_{i=N_L+1}^{N_L+N_R} F_i^H L_i \sin(\alpha_i - \theta_G) \\ - \sum_{i=1}^{N_L} F_i^y L_i \cos(\alpha_i + \theta_G) \\ + \sum_{i=N_L+1}^{N_L+N_R} F_i^y L_i \cos(\alpha_i - \theta_G) = 0 \end{aligned} \quad (19)$$

where  $I$  and  $\theta_G$  are moment of inertia and rotational angle response vector at mass center, and  $N_L$ ,  $N_R$  are total number of LRB in left and right side from mass center position, and  $L_i$ ,  $\alpha_i$  represent distance and geometric angle from mass center to  $i$ th LRB location respectively.

The restoring force exerted at LRB can be expressed using the viscous damping and the stiffness of LRB itself as follows;

$$F_i^H = C_i^H \dot{x}_i + K_i^H x_i \quad (20)$$

$$F_i^y = C_i^y \dot{y}_i + K_i^y y_i \quad (21)$$

where  $C_i$  and  $K_i$  are viscous damping and stiffness of  $i$ th LRB respectively.

The responses such as displacement, velocity and acceleration at any point of rigid body superstructure can easily be obtained from the following equations, which use the response results at mass of center.

$$x_j = x_G + p_j (\cos \theta_G - 1) - q_j \sin \theta_G \quad (22)$$

$$y_j = y_G + p_j \sin \theta_G + q_j (\cos \theta_G - 1) \quad (23)$$

$$\dot{x}_j = \dot{x}_G - p_j \sin \theta_G \cdot \dot{\theta}_G - q_j \cos \theta_G \cdot \dot{\theta}_G \quad (24)$$

$$\dot{y}_j = \dot{y}_G + p_j \cos \theta_G \cdot \dot{\theta}_G - q_j \sin \theta_G \cdot \dot{\theta}_G \quad (25)$$

$$\begin{aligned} \ddot{x}_j = \ddot{x}_G - p_j (\cos \theta_G \cdot \ddot{\theta}_G^2 + \sin \theta_G \cdot \ddot{\theta}_G) \\ - q_j (\sin \theta_G \cdot \ddot{\theta}_G^2 - \cos \theta_G \cdot \ddot{\theta}_G) \end{aligned} \quad (26)$$

$$\begin{aligned} \ddot{y}_j = \ddot{y}_G + p_j (-\sin \theta_G \cdot \ddot{\theta}_G^2 + \cos \theta_G \cdot \ddot{\theta}_G) \\ + q_j (\cos \theta_G \cdot \ddot{\theta}_G^2 + \sin \theta_G \cdot \ddot{\theta}_G) \end{aligned} \quad (27)$$

where  $p_j$  and  $q_j$  are the  $x$  and  $y$  coordinates to calculate the responses measured from original

point of mass center in state of no excitation.

### 3.1.2 Multi-DOF model

The general equations of motion for multi-dof model shown in Fig. 4(b) can be expressed as follows;

$$\begin{aligned} m_1 \dot{x}_1 + c_1 (\dot{x}_1 - \dot{x}_0 - h_1 \dot{\theta}) + k_1 (x_1 - x_0 - h_1 \theta) \\ = -m_1 \dot{x}_g \end{aligned} \quad (28)$$

$$\begin{aligned} m_0 \dot{x}_0 - c_1 (\dot{x}_1 - \dot{x}_0 - h_1 \dot{\theta}) - k_1 (x_1 - x_0 - h_1 \theta) \\ + \sum_{i=1}^N F_i^H = -m_0 \dot{x}_g \end{aligned} \quad (29)$$

$$\begin{aligned} \sum_n I_n \ddot{\theta} + \{c_1 (\dot{x}_1 - \dot{x}_0 - h_1 \dot{\theta}) - k_1 (x_1 - x_0 - h_1 \theta)\} h_1 \\ - \sum_i F_i^H h_0 + \sum_{i=1}^N L_i^2 (C_i^y \dot{\theta} + K_i^y \theta) = 0 \end{aligned} \quad (30)$$

$$\sum_n m_n \dot{y} + \sum_{i=1}^N (C_i^y \dot{y} + K_i^y y) = -\sum_n m_n \dot{y}_g \quad (31)$$

$$F_i^H = C_i^H \dot{x}_0 + K_i^H x_0 \quad (32)$$

where subscript  $n$  represents the floor number, and  $x_n$  ( $n=0, 1$ ) is the relative displacement vectors of each floor, and  $y$ ,  $\theta$  are a vertical displacement and a rotational angle vector, and  $m_n$ ,  $I_n$  ( $n=0, 1$ ) are a total mass and moment of inertia for each floor, and  $F_i^H$  is a horizontal restoring force of  $i$ th LRB.

For the solution of above Eqs. (12)–(16), the Runge–Kutta numerical algorithm is used. To apply this algorithm, the original vectors will be transformed to make a second order equation to first order equation as follows;

$$z = \{x_0, y_0, \theta_0, x_1, y_1, \theta_1, \dot{x}_0, \dot{y}_0, \dot{\theta}_0, \dot{x}_1, \dot{y}_1, \dot{\theta}_1\}^T \quad (33)$$

$$\dot{z} = \{\dot{x}_0, \dot{y}_0, \dot{\theta}_0, \dot{x}_1, \dot{y}_1, \dot{\theta}_1, \ddot{x}_0, \ddot{y}_0, \ddot{\theta}_0, \ddot{x}_1, \ddot{y}_1, \ddot{\theta}_1\}^T \quad (34)$$

where  $y_0 = y_1 = y$ ,  $\dot{y}_0 = \dot{y}_1 = \dot{y}$ ,  $\ddot{y}_0 = \ddot{y}_1 = \ddot{y}$ ,  $\theta_0 = \theta_1 = \theta$ ,  $\dot{\theta}_0 = \dot{\theta}_1 = \dot{\theta}$ , and  $\ddot{\theta}_0 = \ddot{\theta}_1 = \ddot{\theta}$ .

## 3.2 Examples of application

### 3.2.1 Experiments of seismically isolated structure

To investigate the isolation characteristics of a seismically isolated structure, the shaking table tests for the reduced model using four LRBs, which support four corners of the basemat as shown in Fig. 5, are carried out. In the schematic drawing of Fig. 5, the slab (6.0 tons) is supported

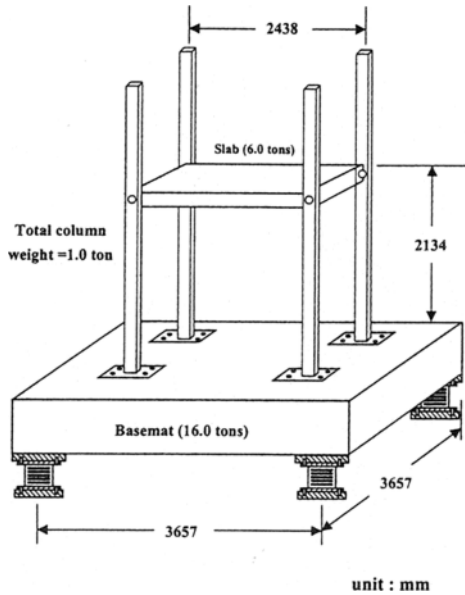


Fig. 5 Schematic shape of a seismically isolated structure for shaking table tests.

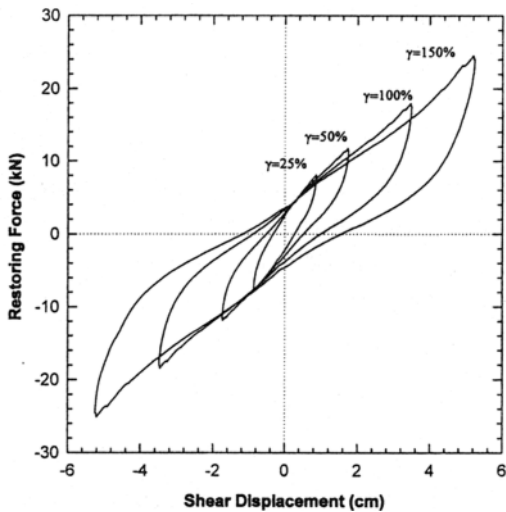


Fig. 6 Hysteretic characteristics of LRB using the loading rate 0.05Hz.

by four columns which are anchored at the basemat (16.0 tons). The total weight of the superstructure is about 23 tons.

The LRBs used in seismic isolation are the reduced 1/8 scale model. The outer and inner diameter of LRB is 144 mm and 19 mm, respectively. The rubber and steel plate thickness is 1.2 mm and 1.7 mm and the number of rubber plates is 29. Fig. 6 shows the hysteretic characteristics of

Table 1 Characteristics of LRB obtained from experiments

Strain $\gamma$ (%)	Stiffness $K_{eq}$ (ton/mm)	Damping Ratio	
		$\xi_{eq}$	Max. Disp. (mm)
25	0.09034	0.16	8.75
50	0.06679	0.15	17.5
100	0.05185	0.13	35.0
150	0.4717	0.12	52.5

LRB obtained from quasi-static experiments of LRB itself with vertical load 4.5 tons and loading rate 0.05Hz for shear strain 25%, 50%, 100% and 150%. Table 1 gives the equivalent stiffness and damping of LRB evaluated for Fig. 6. As shown in the table, the LRB used in experiments has high damping characteristics from 12% to 16%.

The input table motion used in experiments is 1940 El-Centro NS. The time interval of the input table motion is determined as 7.071ms considering the scale factor, 1/8 for original data of 0.02 seconds.

### 3.2.2 Shear displacement responses of LRB

To investigate the shear displacement responses of LRB for earthquakes, the shaking table tests are carried out for SIS shown in Fig. 5, which are supported by four LRBs at each corner position of the basemat. The specifications of the shaking table system are described in Table 2.

For analysis model of LRB derived in Eqs. (20) and (32), the horizontal stiffness can be calculated from Eq. (1). Using design data of  $D_o = 144\text{mm}$ ,  $D_i = 19\text{mm}$ ,  $t_R = 1.2\text{mm}$ ,  $t_S = 1.7\text{mm}$ ,  $n_R = 29$ ,  $G = 0.78\text{MPa}$ ,  $E = 1.49\text{GPa}$ , and  $\chi = 0.5$ , the horizontal design stiffness of each LRB is calculated 365 kN/m, which gives a seismic isolation frequency 1.3Hz. Damping used in analyses is assumed as viscous damping 14%, which is the averaged equivalent damping value obtained from LRB tests in a range of 25% to 150% shear strain range.

For the input acceleration time history in numerical analyses, the shaking table motions are used, which are directly measured in experiments.

**Table 2** Specifications of the shaking table system used in experiments.

Description	Specification
• Table Size	4.0m × 4.0m
• Specimen Weight	30 tons
• Control Method	Electrohydraulic servo control
• System Scaling	10 Vcd with ranges at 100% and 200%
• Excitation Axes	X, Y, Z, Rx, Ry, Rz
• Maximum Dynamic Displacement	
X and Y axis	±100 mm
Z axis	±67 mm
• Maximum Velocity	
X and Y axis	±75 cm/s
Z axis	±50 cm/s
• Maximum Acceleration (with 30ton specimen)	
X and Y axis	±1.5 g
Z axis	±1.0 g
• Control Degree of Freedom	6 DOF
• Allowable Over Turning Moment	110 ton-m
• Allowable Off Center Load	20 ton-m
• Data Acquisition	64 Channels

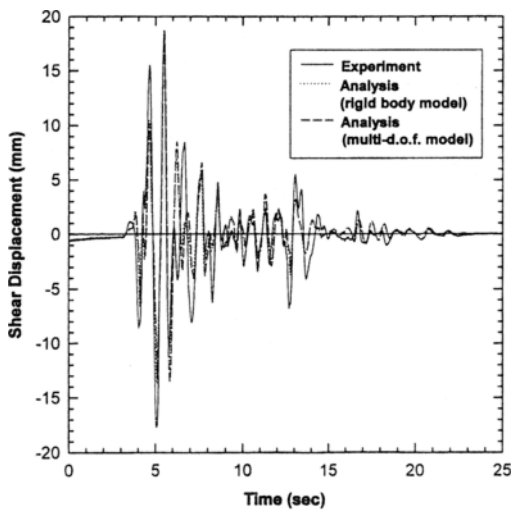


**Fig. 7** Dynamic shear displacement responses of LRB for 0.42g table motion.

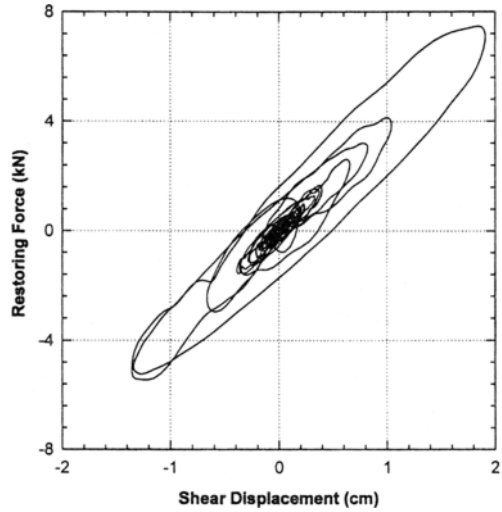


**Fig. 8** Analysis results of hysteretic responses of LRB (14% damping, 0.42g).

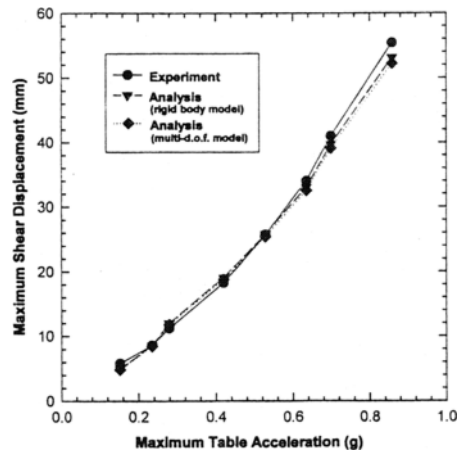


**Fig. 9** Maximum shear displacement responses of LRB.

Fig. 7 shows the time history responses of LRB shear displacement for 0.42g input time history acceleration. In this figure, the time history responses obtained by both experiments and analyses show a very good agreement in global wave form and peak response. Fig. 8 shows the hysteretic responses of LRB obtained from analysis. The maximum restoring force is about 8kN at 20mm shear displacement of LRB. This result is slightly lower than that of experimental results shown in Fig. 6. This is due to the underestimated horizontal stiffness used in analysis.

Fig. 9 shows the maximum peak shear displace-

ment responses of LRB for various input accelerations up to about 0.8g. The results obtained using both rigid body model and multi-d. o. f. model show good agreement with those of experiments throughout all acceleration levels. When we consider the SSE (Safe Shutdown Earthquake) level for nuclear power plant design, the LRB shear displacement at this level is about  $\gamma=40\%$  (14 mm), which is significantly lower than the design shear displacement,  $\gamma=200\%$ . Therefore, it is confirmed that overall SIS using the laminated rubber bearings is so stable for maximum design input acceleration level.

**3.2.3 Variation of seismic isolation frequencies**

In general, the hysteretic behavior of LRB shows that the horizontal stiffness decreases as the maximum shear displacements for each cyclic load increase. Therefore, the seismic isolation frequency is changed according to the input seismic level.

Fig. 10 shows the parameter curves of seismic isolation frequency variation obtained from experimental results. The solid curve in Fig. 10 is produced from the data of the transfer response functions obtained from the shaking table tests of SIS using random excitations and the dotted curve is obtained from a simple equation as  $f_{iso} = (1/2\pi)\sqrt{(K_{eq}/M)}$  using the quasi-static test data of LRB itself shown in Table 1. The results of

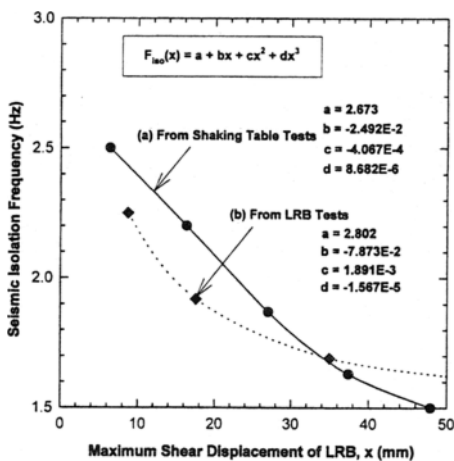


**Fig. 10** Curves of seismic isolation frequency obtained from experiments.

Fig. 10 are in good agreement with general characteristics of the loading rate effects for the high damping LRB.

To investigate the effects of seismic isolation frequency variation on seismic responses of SIS, the parameter equations of seismic isolation frequency are obtained

from shaking table tests

$$f_{iso} = 2.673 - (2.492 \times 10^{-2})x - (4.067 \times 10^{-4})x^2 + (8.682 \times 10^{-6})x^3 \quad (35)$$

from LRB tests

$$f_{iso} = 2.802 - (7.873 \times 10^{-2})x + (1.891 \times 10^{-3})x^2 - (1.567 \times 10^{-5})x^3 \quad (36)$$

where  $x$  is a shear displacement of LRB with unit of  $mm$ .

The horizontal stiffness and damping of LRB used in seismic time history analyses are calculated using a simple equation,  $K_H = M(2\pi f_{iso})^2$ , where  $f_{iso}$  is obtained using the shear displacement data corresponding to the shaking table acceleration level measured in experiments.

**3.2.4 Seismic responses**

The benefit of seismic isolation using LRB is shown in Fig. 11. In these experimental results, the maximum peak acceleration responses at slab for seismic isolation case are significantly reduced than those of non-isolation case. For example of 0.3g table motion, the reduction ratio is about 7.5. This will greatly increase as the table accelera-

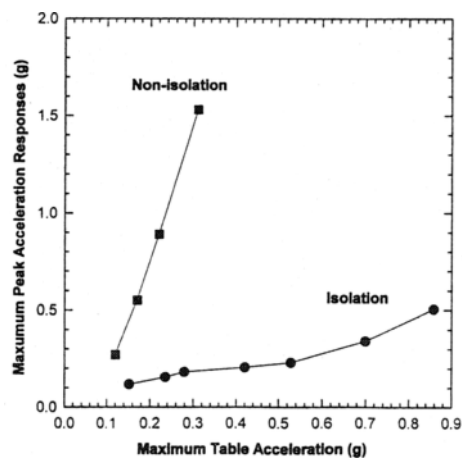


**Fig. 11** Maximum peak acceleration responses at slab obtained from experiments.

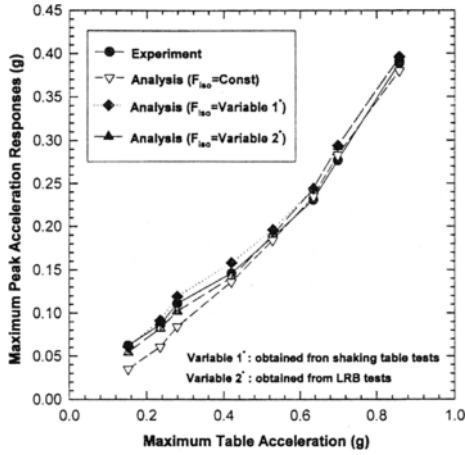


Fig. 12 Maximum peak acceleration responses at basemat.

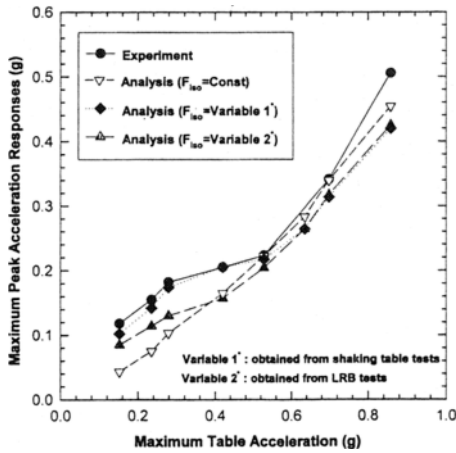


Fig. 13 Maximum peak acceleration responses at slab.

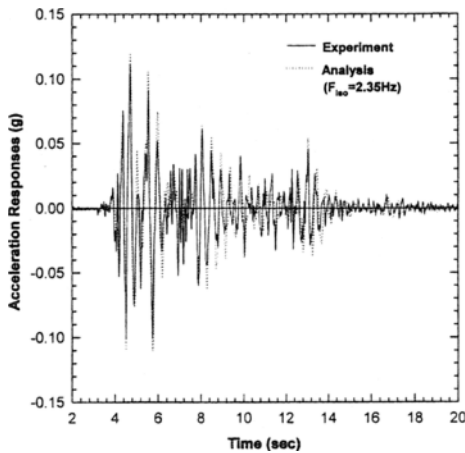


Fig. 14 Acceleration time history responses at basemat for 0.28g table motion.

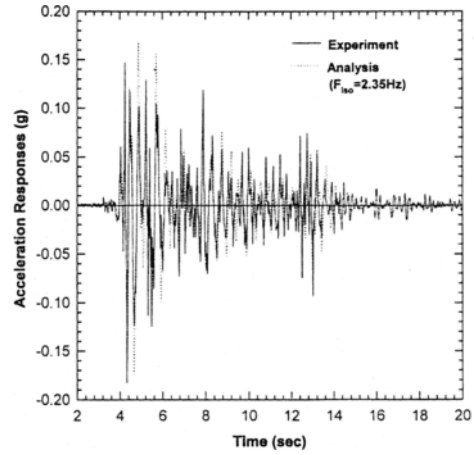


Fig. 15 Acceleration time history responses at slab for 0.28g table motion.

tion levels increase.

Figures 12 and 13 show the maximum peak acceleration responses at basemat and slab. In figures, the numerical analysis results are obtained using the multi-d. o. f. model with and without considering the isolation frequency variations. In figures, we can see that the seismic isolation frequency variations significantly affect the maximum peak acceleration responses. Therefore, it is recommended that the variation of the mechanical characteristics of LRB corresponding to the cyclic shear displacements should be considered in seismic isolation design by analysis.

Figures 14 and 15 show the acceleration time history responses at basemat and slab for 0.28g input table motion. In figures, the overall waveforms of acceleration responses obtained from numerical analyses are in good agreement with those of experiments.

#### 4. Conclusion

When considering the rubber compression effects, the increase of the total rubber height more than the rubber plate thickness in LRB effectively decreases the buckling load.

The seismic responses can be significantly reduced with introducing the seismic isolation design using LRB. From the comparison of the maximum peak acceleration responses obtained from numerical analyses and experiments, it is

verified that the horizontal stiffness variations of LRB should be considered in seismic analysis to get more accurate results.

### Acknowledgment

This project has been carried out under the Nuclear R&D Program by MOST.

### References

- Haringx, J. A., 1948-1949, "On Highly Compressive Helical Springs and Rubber Rods and Their Applications to Free Mountings-Part I, II and III," *Philips Research Reports*.
- Gent, A. N., 1964, "Elastic Stability of Rubber Compression Springs," *Journal of Mechanical Engineering Science*, Vol. 6, No. 4, pp. 318-326.
- Koh, C. G. and Kelly, J. M., 1987, "Effects of Axial Load on Elastomeric Isolation Bearings," *Earthquake Engineering Research Center, University of California, Report No. UBC/EERC* -86/12.
- Koo, G. H., Lee, J. H., Yoo, B. and Ohtori, Yasuki, 1998, "Evaluation of Laminated Rubber Bearing for Seismic Isolation Using Modified Macro-Model with Parameter Equations of Instantaneous Apparent Shear Modulus," *Engineering Structures*, Vol. 21, No. 7, pp. 594-602.
- Forni, M., Martelli, A., et. al., 1994, "Proposal for Design Guidelines for Seismically Isolated Nuclear Plants-Final Report," European Atomic Energy Community and ENEA.
- Koo, G. H. and Ohtori, Y., 1998, "Loading Rate Effects of High Damping Seismic Isolation Rubber Bearing on Earthquake Responses," *KSME International Journal*, Vol. 12, No. 1, pp. 58-66.
- Fujita, T., Fujita, S., Suzuki, S. and Yoshizawa, T., 1987, "Experimental Study of Laminated Rubber Bearings for Earthquake Isolation of Buildings," *Transactions of Japan Society of Mechanical Engineers*, Vol. 53. No. 485, pp. 71-76.